ADVANCED FUNCTIONAL MATERIALS
www.afm-journal.de

Modulating and Accelerating Photolysis of Photoactivatable [2.2]Paracyclophane Aryl Azide in Supramolecular Host for Bioimaging

Xujun Qiu, Eric Pohl, Qianyu Cai, Jasmin Seibert, Yuting Li, Sonja Leopold, Olaf Fuhr, Michael A. R. Meier, Ute Schepers, and Stefan Bräse**

Photolysis of aryl azides offers a versatile approach to achieve more sophisticated functionalization, for instance in the field of chemical biology. In this study, a photoactivatable aryl azide named Pcp-Az is presented that forms three distinct emissive molecules after irradiation. Computational studies unveiled that the photolysis of Pcp-Az in aqueous medium undergoes different reaction channels, leading to the three mentioned distinct products. When the photoreaction is performed using the supramolecular host cucurbit[8]uril(CB8) for Pcp-Az, the reaction is found to be tuned and accelerated. Finally, the potential application of the photoproducts are showcased in bioimaging, and also the time-dependent photoactivating imaging.

1. Introduction

Rational design of photoactivatable fluorophores (PAFs), which can undergo specific photoreaction pathways from non-fluorescent or low fluorescent molecules to immensely emissive dyes, are highly desirable, particularly for biological applications.[1] Fluorescent turn-on processes in living cells have drawn considerable attention for tracking dynamic biological processes, monitoring bioactive molecules, or real-time localization bioimaging.[2] To date, numerous PAFs have been unveiled based on the different photoreaction mechanisms, dominantly including photoisomerization,[3] photoconversion,[4] and photouncaging.[5]

Organic azides have shown wide application possibilities in biological fields, as they can be transferred to the other functional molecules through various reaction pathways such as copper(I)-catalyzed azide-alkyne cycloaddition (CuAAC) click reaction,[6] Staudinger ligation,[7] or reduction to amines.[8] Photolysis of aryl azides has become a burgeoning topic in chemical biology.[9] However, PAFs based on the photolysis of aryl azides in the living cell were rarely reported.[10] This could be due to the extremely active singlet nitrene generated upon the photolysis of azides, resulting in uncontrollable photoreaction pathways.[11] Developing mild and efficient methods to steer the photolysis of aryl azides in chemical biology are urgently wanted.

With the benefits of reactions in a "molecular flask",[12] i.e., reactions within a supramolecular host molecule, we have previously established a novel approach to control the photoreaction pathway of aryl azides within the cavity of cucurbit[7]uril (CB7) to obtain carbolines with excellent selectivity.[13] Our previous results suggest, indeed, that the photolysis of the designed aryl azides in aqueous media results in various photoproducts. On the contrary, when photoreactions were implemented within the CB7 cavity, the reaction pathway was altered to intramolecular C-H amination, selectively forming carbolines with dramatically enhanced fluorescence intensity.[13] With these primary results in mind, we are seeking the potential opportunity to apply this controlled photolysis process in biology.

[2.2]Paracyclophane (PCP), a unique molecule that contains two benzene moieties in a coplanar packing with 3.09 Å of deck distance, which is smaller than Van der Waals distance found

X. Qiu, Q. Cai, J. Seibert, Y. Li, M. A. R. Meier, U. Schepers, S. Bräse
Institute of Organic Chemistry (IOC)
Karlsruhe Institute of Technology (KIT)
Kaiserstrasse 12, 76131 Karlsruhe, Germany
E-mail: ute.schepers@kit.edu; braese@kit.edu
E. Pohl, S. Leopold, U. Schepers
Institute of Functional Interfaces (IFG)
Karlsruhe Institute of Technology (KIT)
Kaiserstrasse 12, 76131 Karlsruhe, Germany
O. Fuhr
Institute of Nanotechnology (INT)
Karlsruhe Institute of Technology (KIT)
Kaiserstrasse 12, 76131 Karlsruhe, Germany
O. Fuhr
Karlsruhe Nano Micro Facility (KNMFi)
Karlsruhe Institute of Technology (KIT)
Kaiserstrasse 12, 76131 Karlsruhe, Germany
M. A. R. Meier, S. Bräse
Institute of Biological and Chemical Systems – Functional Molecular Systems (IBCS-FMS)
Karlsruhe Institute of Technology (KIT)
Kaiserstrasse 12, 76131 Karlsruhe, Germany

The ORCID identification number(s) for the author(s) of this article can be found under https://doi.org/10.1002/adfm.202401938

DOI: 10.1002/adfm.202401938

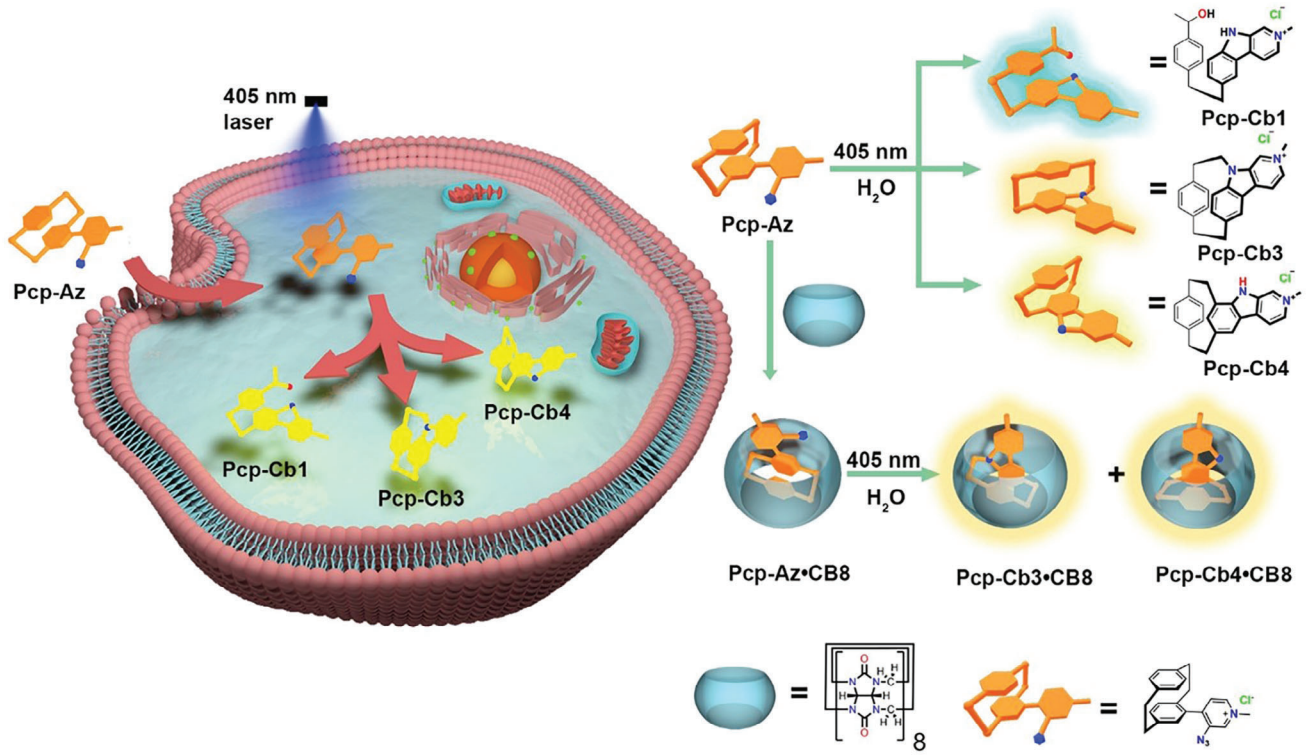

Scheme 1. Schematic illustration of photoactivatable aryl azide (**Pcp-Az**) "turn on" emission in a living cell (left) and modulating the photoreaction of the **Pcp-Az** with CB8 as reaction chamber (right).

between graphite layers (3.35 Å), and enables robust transannular electronic communication between the benzene decks. PCP molecules have shown intriguing photophysical properties, making them promising candidates for fabricating optical materials.[14] In this study, we designed a novel photoactivatable aryl azide (**Pcp-Az**) with PCP as a core structure, which can undergo three different reaction channels in the aqueous medium, resulting in three distinctive emissive products (**Pcp-Cb1**, **Pcp-Cb3**, **Pcp-Cb4**, **Scheme 1**). We showcased the modulating and accelerating of the photolysis of **Pcp-Az** within the cavity of cucurbit[8]uril (CB8) from low emissive aryl azide to highly fluorescent carbolines. In the end, we have successfully applied the photoreaction of the aryl azide in living cells to achieve optical imaging, highlighting the potential of our photoactivatable system.

2. Results and Discussion

2.1. Design and Strategy

The intriguing photophysical properties of carboline derivatives have been disclosed in various applications.[15] Indeed, our previously reported carboline derivative shows excellent emission properties in both aqueous medium and the solid state.[13] We were thus curious about the photophysical properties of a derivative where one of the benzene rings is substituted with a [2.2]paracyclophane system. To synthesize the desired PCP-carboline, we thus applied our reported method by photolyzing PCP aryl azide (**Pcp-Az**) in the supramolecular host CB8.[13] The synthesis of **Pcp-Az** is straightforward, comprising the following steps: 1) synthesis of the stable [2.2]paracyclophane trifluoroborate salt from 4-bromo[2.2]paracyclophane via a pinacol boronic ester route;[16] 2) palladium-catalyzed Suzuki cross-coupling reaction to obtain amino pyridyl [2.2]paracyclophane; 3) azide preparation from amino pyridyl [2.2]paracyclophane to yield azido pyridyl [2.2]paracyclophane;[17] 4) methylation of azido pyridyl [2.2]paracyclophane and ion exchange resulting the desired **Pcp-Az**. The synthesis and characterization details are shown in the supporting information (Figures S1–S4, Supporting Information).

2.2. Photolysis of Pcp-Az in and within the CB8 Cavity

The photolysis of **Pcp-Az** was initially investigated in water using 405 nm LEDs for irradiation. After the irradiation, new peaks in the ^{1}H NMR spectra emerged (Figure S5, Supporting Information). Three identical main peaks referring to methyl protons in the aliphatic region at 4.53, 4.45, and 4.43 ppm were observed in approximately 1:1:1 ratio. To gain further information about the photoreaction products, Liquid Chromatography–Mass Spectrometry (LC–MS) was utilized to track the reaction mixtures and their corresponding mass. Indeed, three majority fractions were observed at retention times of 3.7, 3.9, and 4.1 min corresponding to molecular weights of 331.30, 313.30, and 313.31 g mol^{-1}, respectively (Figure S6, Supporting Information). Our previous study suggested that a nucleophilic attack of water can occur when the photoreaction of aryl azide is performed in aqueous condition, leading to an azepine product.[13] With this in mind, we are able to conclude that the molecular weight of one product

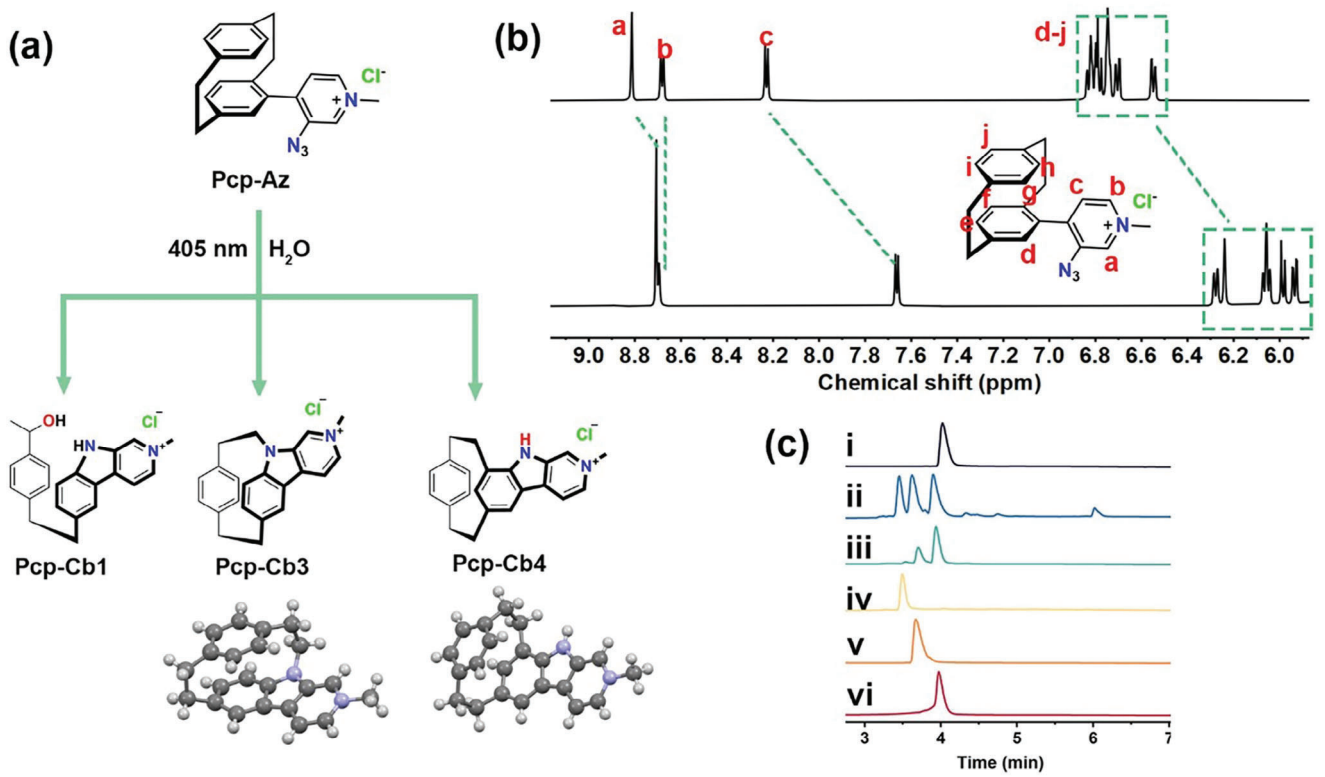

Figure 1. a) Structures of photoreaction products from **Pcp-Az**, and molecular structures of **Pcp-Cb3** and **Pcp-Cb4** (counter ions were omitted for clarify, crystal details can be seen in the Supporting Information); b) ^{1}H NMR spectra (500 MHz, D_2O, 298 K) of **Pcp-Az** and **Pcp-Az**·CB8 (1:1, 0.5 mM), partial region is shown, for full spectra see Figure S29 (Supporting Information); c) LC-MS spectra of i) **Pcp-Az**; ii) **Pcp-Az** after photoreaction in bulk water; iii) **Pcp-Az**·CB8 after photoreaction; iv) **Pcp-Cb1**; v) **Pcp-Cb3**; vi) **Pcp-Cb4**.

from photolysis of **Pcp-Az**, after losing nitrogen and the addition of water, shows a molecular weight of ≈331 g mol^{-1}, fitting to the first fraction from LC-MS. Another possible reaction pathway can involve a C-H amination, yielding a carboline derivative with a molecular weight of ≈313 g mol^{-1}, which is comparable to what we observed from the LC-MS results. Interestingly, the latter fractions from LC-MS with the same molecular weight suggest two isomers could emerge during the photoreaction.

To systematically study the formation of the three products from the photolysis of **Pcp-Az**, we separated the reaction mixture via Preparative Reversed-Phase High-Performance Liquid Chromatography (RP-HPLC). The NMR studies of these three species can be seen in the supporting information (Figures S7–S22, Supporting Information). For the first fraction, at a retention time of 3.7 min, unexpected signals in the aliphatic range were observed compared to the typical signals from the PCP ethylene bridge, indicating a disintegration of the ethylene bridge during the photolysis of the **PCP-Az**. With the characterization from the 2D NMR spectra (Figures S7–S12, Supporting Information), the structure (**Pcp-Cb1**) could be determined, which can be seen in **Figure** 1a. For the second fraction at a retention time of 3.9 min, the ethylene bridge signals were still observed in the NMR spectra (Figures S13–S17, Supporting Information), suggesting an intact PCP structure after the photoreaction process. Interestingly, upfield-shifted aromatic protons were observed at ≈5.50 and 4.95 ppm (Figure S13, Supporting Information), indicating a shielded aromatic ring system could have formed. The third product was also observed with an intact ethylene bridge (Figures S18–S22, Supporting Information) as well as the shielded aromatic ring from 5.23–5.84 ppm, which could be due to the rearrangement of PCP decks. For comparison, we synthesized **Pcp-Cb1** utilizing a traditional approach involving Buchwald-Hartwig cross-coupling, C—H activated cyclization, methylation, and ion exchange (Figures S23–S26, Supporting Information). Indeed, the NMR spectra of **Pcp-Cb1** indicates none of these two C—H aminated products were the desired structure.

Unfortunately, many efforts failed to grow a single crystal from the obtained first and second products. Therefore, we exchanged the counter ion to PF_6^- and afterward, crystallization and signal crystal structure evaluation was successful for the second product, **Pcp-Cb3**, which can be seen in Figure 1a, Figure S27, and Table S1 (Supporting Information). Unlike the original PCP structure, an expanded deck system was observed with a maximum distance of 7.80 Å from one ethylene proton to the diagonal ethylene proton (Figure S27, Supporting Information). A single crystal was also successfully obtained for the third product **Pcp-Cb4** (Figure 1a; Figure S28, and Table S2, Supporting Information). Indeed, a migration of the ethylene bridge was observed, resulting in a maximum distance of 7.01 Å from one ethylene proton to the diagonal ethylene proton.

As has been studied previously,[14c] the CB host can efficiently alter the reaction pathway upon photolysis of aryl azide and PCP molecules, which can be complementarily accommodated within the CB8 cavity forming a 1:1 complex with a remarkable binding

constant. Therefore, to investigate the possibility of CB8 in modulating the photolysis of **Pcp-Az**, we initially explored the binding performance of **Pcp-Az** with CB8 by ^{1}H NMR. As shown in Figure 1b and Figure S29 (Supporting Information), as an equimolar amount of CB8 was added to **Pcp-Az** in the D_2O, protons in the aromatic and ethylene range were observed significantly upfield shifted, suggesting encapsulation of **Pcp-Az** within the CB8 cavity. The formation of a 1:1 host-guest complex was evidenced by electrospray ionization (ESI) mass spectrometry, where a mass-to-charge ratio (m/z) of 1669.5964 for [Pcp-Az+CB8]$^+$ was observed (Figure S30, Supporting Information).

The binding constant of **Pcp-Az** with CB8 was studied with a well-established competitive binding assay,[18] where memantine hydrochloride (Mem) was utilized as a competitive guest with a binding constant of 8.28 (± 0.38) × 10^{12} M^{-1}. As shown in Figure S31 (Supporting Information), as an excess of Mem was added to the **Pcp-Az** and CB8 mixtures, two distinct proton signals emerged in ^{1}H NMR at 5.54 and 5.47 ppm, related to **Pcp-Az**·CB8 and Mem·CB8, respectively. The binding constant thus can be calculated as (4.05 ± 0.57) × 10^{12} M^{-1} using the binding equations, which indicates a stable host-guest complex system.

Photolysis of **Pcp-Az**·CB8 was performed under the same condition as for photoreaction of **Pcp-Az** in water. Two peaks at 4.65 and 4.52 ppm referring to methyl protons were observed by ^{1}H NMR after the photoreaction (Figure S32, Supporting Information), suggesting that two main products were formed when the photolysis of **Pcp-Az** was performed in the presence of CB8 instead of three without CB8. The LC-MS chromatograms from the reaction mixtures also indicate two main products formed, matching **Pcp-Cb3** and **Pcp-Cb4** (Figures 1c; Figure S33, Supporting Information), while the nucleophilic addition of water was prevented. Interestingly, a lower ratio between **Pcp-Cb3** and **Pcp-Cb4** was observed by NMR as well as LC-MS, which could be due to the smaller and more compatible size products being more favorable within the limited CB8 cavity.

2.3. Density Functional Theory (DFT) Calculation

The photolysis of aryl azides usually undergoes the expulsion of a nitrogen molecule with the formation of an active nitrene species, which can go through different reaction channels depending on the reaction conditions. In this study, three different products were formed from three different reaction pathways in water. Based on our previous results,[13] we suggested the following reaction mechanism (**Figure 2a**). After losing N_2 upon irradiation, a nitrene species can be formed (**Im1**), which tends to attack the PCP moiety forming an intermediate with a five-membered ring (**Im2**). The subsequential re-aromatization leads to a bond break between the aryl and ethylene bridge, offering three reaction pathways: delocalization of the positive charge, generating carbocation-like intermediates Im3$^+$ and Im4$^+$, followed by nucleophilic attack of a water molecule, leading to **Pcp-Cb1**; in situ generation of a diradical, followed by migration of ethylene bridge in two directions, either 2) forming **Pcp-Cb3** directly, or 3) forming the carboline product followed by a 1,3-sigmatropic rearrangement. Experimentally, no sign of forming **Pcp-Cb2** was observed.

To gain more insights into these possible transformations, DFT calculations were performed at the B3LYP/6-31 G(d,p) level as implemented in the Gaussian 16 program package.[19] The Gibbs free energy profile of the possible reaction intermediates is shown in Figure 2b. The photolysis of azide has an activation energy of 30.4 kcal mol^{-1}, leading to a nitrene intermediate. In the case of singlet nitrene **Im1**, this step is exothermic and the reaction free energy is 37.6 kcal mol^{-1}. After the ethylene bridge breakage induced by delocalization of the positive charge, the carbocation **Im3$^+$** is formed, which can be converted to **Im4$^+$** with an energy gain of 6.5 kcal mol^{-1} through a 1,2-H shift. The stabilized styrene-like cation **Im4$^+$** can be further attacked by water, forming the energetically stable product **Pcp-Cb1** with a total energy gain of 100.6 Kcal/mol. This step can also undergo a radical mechanism. Here, we only showcase one possible reaction pathway for forming the open-chained product **Pcp-Cb1**. For reaction pathways, in which water molecules are not involved, which is also the case for reactions conducted in the CB8 cavity (Figure S34a, Supporting Information), **Im2** undergoes homolytic breakage. The in situ formation of a biradical explains the short reaction time and the even distribution of products **Pcp-Cb3** and **Pcp-Cb4**. In this case, Im2 either binds the neighbor nitrogen atom and forms product **Pcp-Cb3**, which brings an energy gain of 88.8 Kcal mol^{-1}or two steps of rearrangement to a lower energy product **Pcp-Cb4**, located at −90.6 Kcal mol^{-1} of the reaction energy profile. The similar energies of **Pcp-Cb1**, **Pcp-Cb3**, and **Pcp-Cb4** indicate why the three species are obtained in around a 1:1:1 ratio after the photoreaction of **Pcp-Az**.

To unveil the reason why **Pcp-Cb2** was observed neither in the bulk water nor within the CB8 void, we also computed the possible reaction intermediate energies upon the reaction (Figure 2b; Figure S34a,b, Supporting Information). The transition state **TS2'** was calculated with an energy barrier of 38 Kcal mol^{-1}. It is 8.2 Kcal mol^{-1} higher than **TS2**, which leads to an intermediate of more substituted carbon atom **Im2**. The reaction energy within the CB8 cavity is shown in Figure S34 (Supporting Information), the energy barrier of the final products **Pcp-Cb3**·CB8 and **Pcp-Cb4**·CB8 were found comparable to the products **Pcp-Cb3** and **Pcp-Cb4** formed in the bulk water.

2.4. Photophysics of the Photolysis of the PCP-Az and CB8 Assembly

Next, we studied the photolysis process of **PCP-Az** and **Pcp-Az**·CB8 in phosphate-buffered saline (PBS) solution by UV–vis and emission spectroscopy. As shown in Figure S35 (Supporting Information), upon irradiation, absorption of the reaction mixtures was observed to change gradually. The maximum absorbance at 344 nm from **PCP-Az** decreased and two new signals at 257 and 311 nm emerged at the same time (Figure S35a, Supporting Information). A similar behavior was also observed during the photoreaction of Pcp-Az·CB8, where absorbance at 357 nm decreased and three new absorbance maxima appeared at 264, 326, and 402 nm, respectively (Figure S35b, Supporting Information). This phenomenon is comparable to our previously observed carboline formation process within the CB host. [13] Photoluminescence (PL) intensity upon the photolysis of **PCP-Az** and **Pcp-Az**·CB8 was observed to significantly

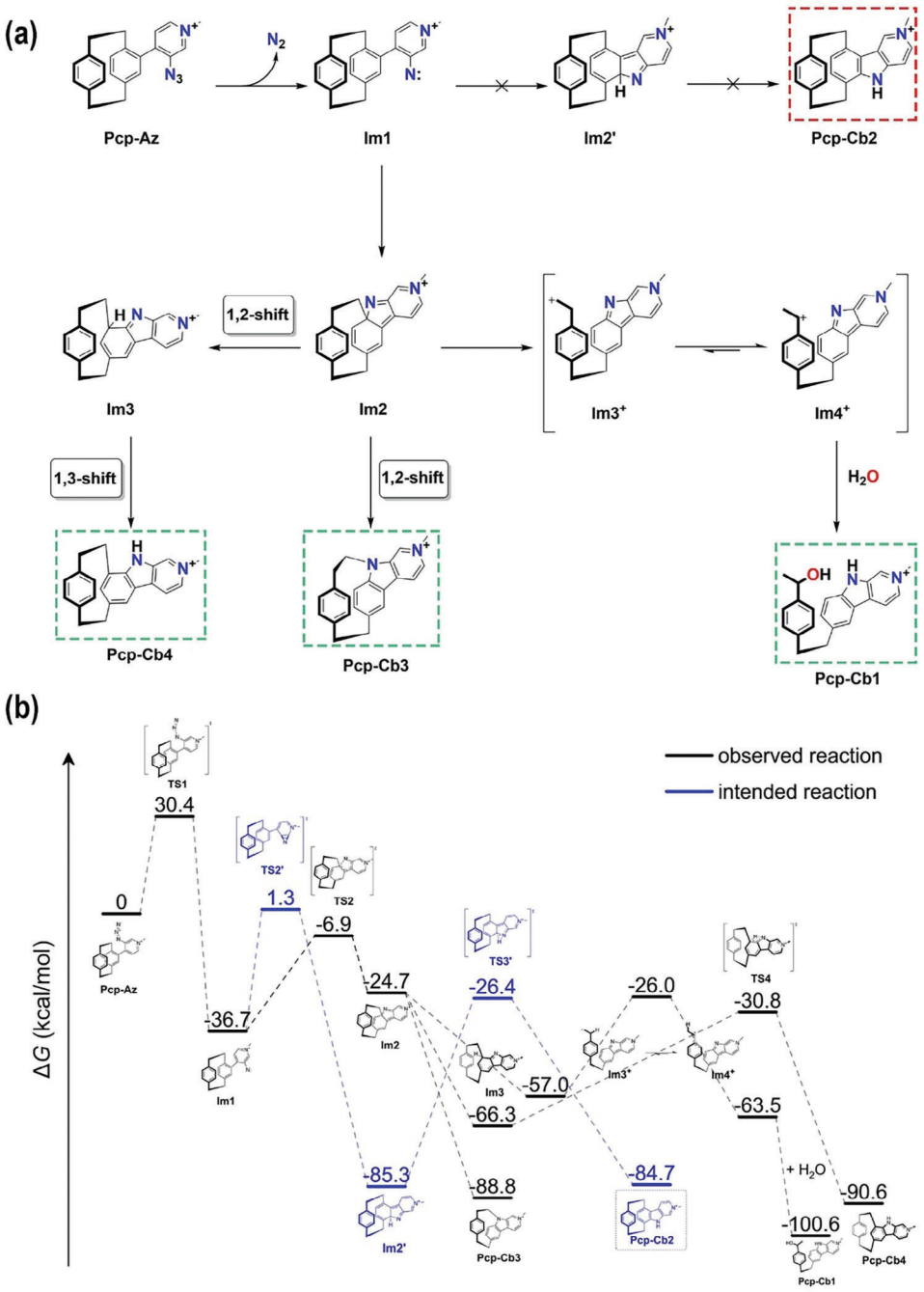

Figure 2. a). Proposed photoreaction mechanism of **Pcp-Az** in water; b) Calculated Gibbs free energy of the possible intermediates. All structures were optimized at the B3LYP /6-31G(d,p) level of DFT with Grimme's D3 diffusion corrections using the software package Gaussian 16.[19]

increase (**Figure 3**). As shown in Figure 3a, the emission intensity at $\lambda_{493\,nm}$ increased 52-fold after the photoreaction compared to the weak emission of **PCP-Az** (Figure 3a). For **Pcp-Az**·CB8, an eight-fold enhancement at λ_{496} nm was observed after the completion of the reaction, along with a hypsochromic shift of maximum emission wavelength from 520 to 496 nm (Figure 3b). Surprisingly, CB8 also played a role as a reaction accelerator when the photolysis was performed within the CB8 cavity with a reaction time of ≈50 s compared to 190 s in water, suggesting the reaction efficiency is almost four times than the reaction of without the CB8. Such an enhancement effect was not found in our previous study, which could be due to the fact that the confined space from CB8 sterically restricts the ring expansion process upon the photoreaction, resulting in the acceleration of the reaction.

We further studied the photophysical properties of the photoreaction products and their host-guest complexes with CB8 in PBS. As shown in Figure S36 (Supporting Information) and **Table 1**, upon complexation of **Pcp-Az** with CB8, bathochromic

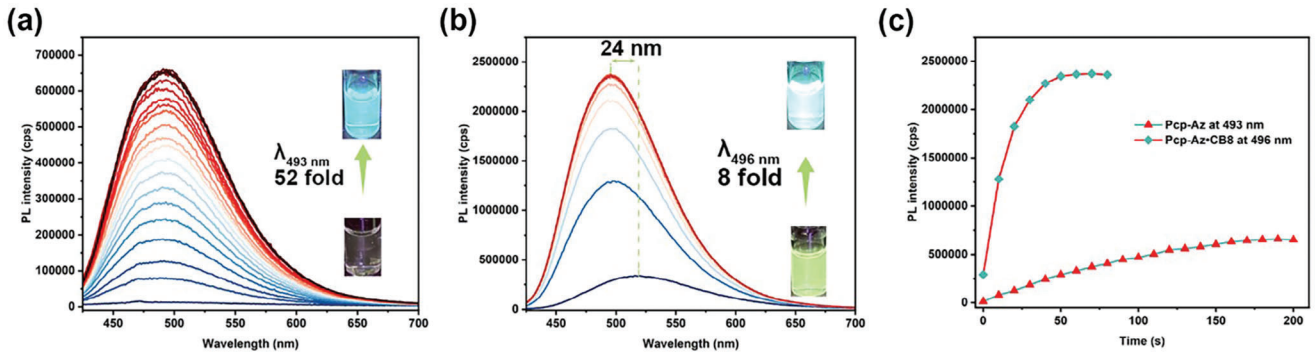

Figure 3. a) The emission spectra of **Pcp-Az** upon the irradiation (20 μM, excitation at 405 nm, entrance and exit slit: 2 nm); b) emission spectra of **Pcp-Az**·CB8 upon the irradiation (20 μM, excitation at 405 nm, entrance and exit slit: 2 nm); c) PL intensity of **Pcp-Az** at 493 nm and **Pcp-Az**·CB8 at 496 nm against time upon the irradiation. The emission spectra were measured in PBS buffer solutions (pH 7.4, 298 K).

shifts in both absorbance and emission were observed, which could attributed to the conformation and the change of the local environment polarity during the migration of the **Pcp-Az** from the water to the hydrophobic cavity of CB8.[20] At the same time, the luminescence quantum yields (QY) were found significantly enhanced (Table 1), which was beneficial from the hydrophobic void form CB8 can minimize the energy decay from molecular rotation and prevent the attack from water. Interestingly, **Pcp-Cb1** showed the highest QY (44.1%) among the three photoproducts. Elevated QY was also observed when **Pcp-Cb3** and **Pcp-Cb4** were internalized within the CB8 cavity at 41.7% and 35.5%, compared to the bulk solution at 18.3% and 16.3%, respectively.

DFT calculations were performed to further characterize the ground state orbital contribution and the electronic energy of the highest occupied molecular orbital (HOMO) and the lowest unoccupied molecular orbital (LUMO) of the PCP fluorophores. As depicted in Figure S37a (Supporting Information), the HOMO and LUMO energy level of Pcp-Az were found −5.12 and −9.83 eV with a HOMO-LUMO gap of 4.72 eV, respectively. However, the HOMO-LUMO gaps of the photoproducts were increased to 6.10 eV for Pcp-Cb1, 5.71 eV for Pcp-Cb3, and 5.98 eV for Pcp-Cb4, respectively. With these results in mind, we then calculated the absorption and fluorescence of the above molecules (Figure S37b,c, Supporting Information), which are despite the blueshift comparable to the experimental results (Figure S36, Supporting Information).

Table 1. The summary of the photophysical properties of **Pcp-Az** and photoproducts.

Compounds[a)]	λ_{Abs} [nm]	λ_{em} [nm]	Φ_{PL} [%]
Pcp-Az	344	489	1.1
Pcp-Az·CB8	357	520	8.6
Pcp-Cb1	258, 309, 384	472	44.1
Pcp-Cb3	256, 279, 333, 424	521	18.3
Pcp-Cb4	265, 320, 391	511	16.3
Pcp-Cb3·CB8	259, 281, 336, 426	490	41.7
Pcp-Cb4·CB8	271, 326, 398	492	35.5

[a)] Abbreviations: λ_{abs} = absorption maximum, λ_{em} = emission maximum, Φ_{PL} = photoluminescence quantum yield; The absorption and emission spectra were measured in PBS buffer solutions (pH 7.4, 20×10^{-6} M, 298 K).

2.5. Application of the Photoactivatable Pcp-Az in Bioimaging

Despite the high photophysical performance of the PCP derivatives in material science, only a few biological applications were reported,[21] which could be due to their poor solubility in water. Considering the above results, we were eager to investigate potential applications of novel PCP molecules in live cell imaging. In this context, the higher QY of the PCP-CB8 complex is especially interesting. To test the suitability, we first performed cytotoxicity tests using HeLa cells with different concentrations (5 and 10 μM) of the 7 PCP fluorophores. The MTT assay results in Figure S38 (Supporting Information) indicate that the obtained PCP fluorophores exhibit low toxicity (LD50 > 10 μM) in HeLa cells.

Furthermore, we performed cell imaging using the tested PCP fluorophores at a concentration of 5 μM (**Pcp-Cb1**, **Pcp-Cb3**, **Pcp-Cb4**, **Pcp-Cb3**·CB8, **Pcp-Cb4**·CB8). As shown in **Figure** 4a, all studied fluorophores were taken up via endocytosis mainly accumulating in endosomal vesicles. **Pcp-Cb3** and **Pcp-Cb3**·CB8 show endosomal escape leading to a cytosolic arrangement. While the CB8 cavity has no effect on the biocompatibility and the intracellular accumulation of **Pcp-Cb3** and **Pcp-Cb4** (Figure 4a; Figure S39, Supporting Information).

We were then intrigued by the photoreaction performance of **Pcp-Az** and **Pcp-Az**·CB8 within cellular environments. Therefore, we investigated the photoactivation behaviors of **Pcp-Az** and **Pcp-Az**·CB8 by incubating HeLa cells with 5 μM of each fluorophore. Imaging was performed using time-dependent confocal fluorescence microscopy. In Figure 4b,c, the initial state (0 s) for the 5 μM **Pcp-Az** sample reveals a weak fluorescence. Upon the irradiation at 405 nm fluorescence (410–550 nm) gradually increased, reaching a saturated state after 60 s. Moreover, **Pcp-Az** shows colocalization with perinuclear vesicles and the cytosol assuming endocytic uptake and endosomal escape. This aligns well with the intracellular colocalization of the corresponding activated fluorophores **Pcp-Cb1**, **Pcp-Cb3**,and **Pcp-Cb4**. In contrast, when coupled to the CB8 cavity no time-dependent increase of fluorescence for **Pcp-Az**·CB8) was observed within the cells

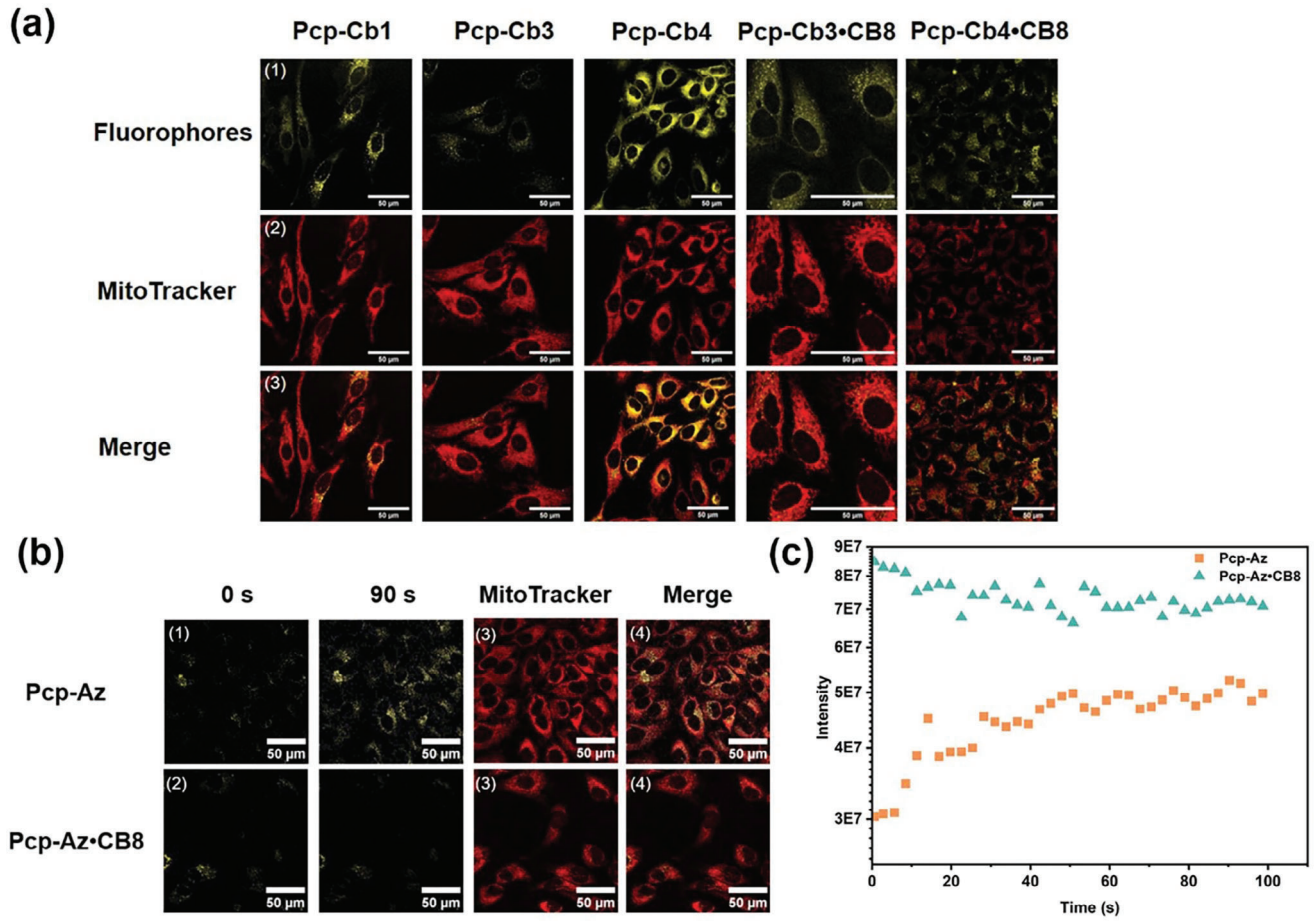

Figure 4. a) Confocal imaging of Hela cell stained with 1) **Pcp-Cb1**, **Pcp-Cb3**, **Pcp-Cb4**, **Pcp-Cb3**·CB8, **Pcp-Cb4**·CB8 (5 μM), and 2) Mitotracker Red, and 3) merged images of (1) and (2); b) confocal imaging of Hela cell stained with 1) **Pcp-Az** and **Pcp-Az**·CB8 (5 μM) at 0 and 60 s, and 2) Mito-Tracker Red, and 3) merged images of (1) and (2); c) the relative intensity upon the irradiation time increased of **Pcp-Az** and **Pcp-Az**·CB8 (5 μM) in Hela cell.

(Figure 4b,c). This lack of enhancement might be attributed to the rapid photoreaction within CB8, as the response time from triggering the reaction to the recording of the images was too fast.

3. Conclusion

In conclusion, we present a novel photoactivatable PCP aryl azide (**Pcp-Az**), which can undergo three different reaction pathways and subsequently form three unique molecules (**Pcp-Cb1**, **Pcp-Cb3**, and **Pcp-Cb4**) in around a 1:1:1 ratio. DFT was performed to propose the reaction mechanism. When the photoreaction was performed with **Pcp-Az** inside a CB8 cavity, the reaction channel toward forming **Pcp-Cb1** was suppressed and the relative formation of **Pcp-Cb3** was reduced. Moreover, the reaction with the supramolecular host was found almost four times faster than the reaction in water. The photophysical property studies of the reaction process and the products demonstrated that the obtained new PCP species have significantly improved QY, compared with the starting materials. Finally, we illustrated the application of the new PCP fluorophores for bioimaging of live cells and photoactivatable imaging.

Supporting Information

Supporting Information is available from the Wiley Online Library or from the author.

Acknowledgements

X.Q. acknowledge the support provided by the China Scholarship Council (CSC grant: 202010190002) and the Deutsche Forschungsgemeinschaft (DFG) under Germany's Excellence Strategy – 3DMM2O – EXC-2082/1–390761711. S.L. thankfully acknowledges funding by the Carl Zeiss Foundation-Focus@HEiKA and support by the Deutsche Forschungsgemeinschaft (DFG) under Germany's Excellence Strategy – 2082/1 – 390761711. Prof. H.-A. Wagenknecht (Institute of Organic Chemistry, KIT) is gratefully acknowledged for giving access to some of the photophysics equipment used in this study.

Open access funding enabled and organized by Projekt DEAL.

Conflict of Interest

The authors declare no conflict of interest.

Data Availability Statement

The data that support the findings of this study are available on request from the corresponding author. The data are not publicly available due to privacy or ethical restrictions.

Keywords

[2.2]paracyclophane, aryl azide, bioimaging, cucurbit[n]urils, photoactivatable, photoreaction

Received: January 31, 2024
Revised: February 26, 2024
Published online:

[1] a) K. A. Lukyanov, D. M. Chudakov, S. Lukyanov, V. V. Verkhusha, *Nat. Rev. Mol. Cell Biol.* **2005**, *6*, 885; b) Y. Zhang, Y. Zheng, A. Tomassini, A. K. Singh, F. M. Raymo, *ACS Appl. Opt. Mater.* **2023**, *1*, 640.

[2] a) J. B. Grimm, B. P. English, H. Choi, A. K. Muthusamy, B. P. Mehl, P. Dong, T. A. Brown, J. Lippincott-Schwartz, Z. Liu, T. Lionnet, L. D. Lavis, *Nat. Methods* **2016**, *13*, 985; b) E. A. Halabi, Z. Thiel, N. Trapp, D. Pinotsi, P. Rivera-Fuentes, *J. Am. Chem. Soc.* **2017**, *139*, 13200; c) S. Hauke, A. von Appen, T. Quidwai, J. Ries, R. Wombacher, *Chem. Sci.* **2017**, *8*, 559; d) J. Tang, M. A. Robichaux, K.-L. Wu, J. Pei, N. T. Nguyen, Y. Zhou, T. G. Wensel, H. Xiao, *J. Am. Chem. Soc.* **2019**, *141*, 14699; e) K. Kikuchi, L. D. Adair, J. Lin, E. J. New, A. Kaur, *Angew. Chem., Int. Ed.* **2023**, *62*, 202204745.

[3] a) G. T. Dempsey, M. Bates, W. E. Kowtoniuk, D. R. Liu, R. Y. Tsien, X. Zhuang, *J. Am. Chem. Soc.* **2009**, *131*, 18192; b) M. K. Lee, P. Rai, J. Williams, R. J. Twieg, W. E. Moerner, *J. Am. Chem. Soc.* **2014**, *136*, 14003; c) O. Nevskyi, D. Sysoiev, A. Oppermann, T. Huhn, D. Wöll, *Angew. Chem., Int. Ed.* **2016**, *55*, 12698; d) B. Roubinet, M. Weber, H. Shojaei, M. Bates, M. L. Bossi, V. N. Belov, M. Irie, S. W. Hell, *J. Am. Chem. Soc.* **2011**, *139*, 6611 e) eG. T. Dempsey, J. C. Vaughan, K. H. Chen, M. Bates, X. Zhuang, *Nat. Methods* **2017**, *8*, 1027.

[4] a) Q. Gong, X. Zhang, W. Li, X. Guo, Q. Wu, C. Yu, L. Jiao, Y. Xiao, E. Hao, *J. Am. Chem. Soc.* **2022**, *144*, 21992; b) X. Zhang, D. Guan, Y. Liu, J. Liu, K. Sun, S. Chen, Y. Zhang, B. Zhao, T. Zhai, Y. Zhang, F. Li, Q. Liu, *Angew. Chem., Int. Ed.* **2022**, *61*, 202211767; c) G. Gou, L. Fang, M. Wang, T. Fan, H. Xu, M. Liu, C. Gu, L. Li, *Adv. Optical Mater.* **2023**, *11*, 2300489; d) X. Chen, N. Niu, D. Li, Z. Zhang, Z. Zhuang, D. Yan, J. Li, Z. Zhao, D. Wang, B. Z. Tang, *Adv. Funct. Mater.* **2023**, *33*, 2211571; e) X. Gu, E. Zhao, T. Zhao, M. Kang, C. Gui, J. W. Y. Lam, S. Du, M. M. T. Loy, B. Z. Tang, *Adv. Mater.* **2016**, *28*, 5064; f) C. Xu, H. Zou, L. Hu, H. Shen, H. H. Y. Sung, H. Feng, R. T. K. Kwok, J. W. Y. Lam, L. Zheng, B. Z. Tang, *ACS Mater. Lett.* **2022**, *4*, 1831.

[5] a) V. N. Belov, C. A. Wurm, V. P. Boyarskiy, S. Jakobs, S. W. Hell, *Angew. Chem., Int. Ed.* **2010**, *49*, 3520; b) A. Loredo, J. Tang, L. Wang, K.-L. Wu, Z. Peng, H. Xiao, *Chem. Sci.* **2020**, *11*, 4410; c) A. N. Butkevich, M. Weber, A. R. Cereceda Delgado, L. M. Ostersehlt, E. D'Este, S. W. Hell, *J. Am. Chem. Soc.* **2021**, *143*, 18388; d) A. Aktalay, T. A. Khan, M. L. Bossi, V. N. Belov, S. W. Hell, *Angew. Chem., Int. Ed.* **2023**, *62*, 202302781.

[6] a) N. Z. Fantoni, A. H. El-Sagheer, T. Brown, *Chem. Rev.* **2021**, *121*, 7122; b) C. G. Parker, M. R. Pratt, *Cell* **2020**, *180*, 605; c) B. L. Kenry, *Trends Chem.* **2019**, *1*, 763.

[7] a) C. I. Schilling, N. Jung, M. Biskup, U. Schepers, S. Bräse, *Chem. Soc. Rev.* **2011**, *40*, 4840; b) C. Bednarek, I. Wehl, N. Jung, U. Schepers, S. Bräse, *Chem. Rev.* **2020**, *120*, 4301.

[8] a) L. J. O'Connor, I. N. Mistry, S. L. Collins, L. K. Folkes, G. Brown, S. J. Conway, E. M. Hammond, *ACS Cent. Sci.* **2017**, *3*, 20; b) H. A. Henthorn, M. D. Pluth, *J. Am. Chem. Soc.* **2015**, *137*, 15330; c) J. Sun, Z. Liu, H. Yao, H. Zhang, M. Zheng, N. Shen, J. Cheng, Z. Tang, X. Chen, *Adv. Mater.* **2023**, *35*, 2207733.

[9] Y. Zhang, J. Tan, Y. Chen, *Chem. Commun.* **2023**, *59*, 2413.

[10] a) S. J. Lord, N. R. Conley, H.-l. D. Lee, R. Samuel, N. Liu, R. J. Twieg, W. E. Moerner, *J. Am. Chem. Soc.* **2008**, *130*, 9204; b) S. Xie, G. Proietti, O. Ramström, M. Yan, *J. Org. Chem.* **2019**, *84*, 14520; c) S. H. Liyanage, N. G. H. Raviranga, J. G. Ryan, S. S. Shell, O. Ramström, R. Kalscheuer, M. Yan, *JACS Au* **2023**, *3*, 1017; d) A. V. Anzalone, Z. Chen, V. W. Cornish, *Chem. Commun.* **2016**, *52*, 9442.

[11] M.-L. Tsao, N. Gritsan, T. R. James, M. S. Platz, D. A. Hrovat, W. T. Borden, *J. Am. Chem. Soc.* **2003**, *125*, 9343.

[12] M. Yoshizawa, J. K. Klosterman, M. Fujita, *Angew. Chem., Int. Ed.* **2009**, *48*, 3418.

[13] X. Qiu, Y. Wang, S. Leopold, S. Lebedkin, U. Schepers, M. M. Kappes, F. Biedermann, S. Bräse, *Small* **2023**, 2307318.

[14] a) E. Spuling, N. Sharma, I. D. W. Samuel, E. Zysman-Colman, S. Bräse, *Chem. Commun.* **2018**, *54*, 9278; b) N. Sharma, E. Spuling, C. M. Mattern, W. Li, O. Fuhr, Y. Tsuchiya, C. Adachi, S. Bräse, I. D. W. Samuel, E. Zysman-Colman, *Chem. Sci.* **2019**, *10*, 6689; c) X. Qiu, T. Zheng, M. Runowski, P. Woźny, I. R. Martín, K. Soler-Carracedo, C. E. Piñero, S. Lebedkin, O. Fuhr, S. Bräse, *Adv. Funct. Mater.* **2024**, 2313517.

[15] a) A. Abdurahman, Y. Chen, X. Ai, O. Ablikim, Y. Gao, S. Dong, B. Li, B. Yang, M. Zhang, F. Li, *J. Mater. Chem.* **2018**, *6*, 11248; b) A. Das, S. U. Dighe, N. Das, S. Batra, P. Sen, *Spectrochim. Acta A Mol. Biomol. Spectrosc.* **2019**, *220*, 117099.

[16] D. M. Knoll, S. Bräse, *ACS Omega* **2018**, *3*, 12158.

[17] X. Qiu, J. Brückel, C. Zippel, M. Nieger, F. Biedermann, S. Bräse, *RSC Adv.* **2023**, *13*, 2483.

[18] D. Sigwalt, M. Šekutor, L. Cao, P. Y. Zavalij, J. Hostaš, H. Ajani, P. Hobza, K. Mlinarić-Majerski, R. Glaser, L. Isaacs, *J. Am. Chem. Soc.* **2017**, *139*, 3249.

[19] a) S. Grimme, J. Antony, S. Ehrlich, H. Krieg, *J. Chem. Phys.* **2010**, *132*, 154104; b) G. A. Petersson, A. Bennett, T. G. Tensfeldt, M. A. Al-Laham, W. A. Shirley, J. Mantzaris, *J. Chem. Phys.* **1988**, *89*, 2193; c) G. A. Petersson, M. A. Al-Laham, *J. Chem. Phys.* **1991**, *94*, 6081; d) M. J. Frisch, G. W. Trucks, H. B. Schlegel, G. E. Scuseria, M. A. Robb, J. R. Cheeseman, G. Scalmani, V. Barone, G. A. Petersson, H. Nakatsuji, X. Li, M. Caricato, A. V. Marenich, J. Bloino, B. G. Janesko, R. Gomperts, B. Mennucci, H. P. Hratchian, J. V. Ortiz, A. F. Izmaylov, J. L. Sonnenberg, Williams, F. Ding, F. Lipparini, F. Egidi, J. Goings, B. Peng, A. Petrone, T. Henderson, D. Ranasinghe, et al., Gaussian, Inc., Wallingford CT, **2016**.

[20] D. Sun, Y. Wu, X. Han, S. Liu, *Nat. Commun.* **2023**, *14*, 4190.

[21] a) S. Bestgen, C. Seidl, T. Wiesner, A. Zimmer, M. Falk, B. Köberle, M. Austeri, J. Paradies, S. Bräse, U. Schepers, P. W. Roesky, *Chem. - Eur. J.* **2017**, *23*, 6315; b) J. Skiba, C. Schmidt, P. Lippmann, P. Ensslen, H.-A. Wagenknecht, R. Czerwieniec, F. Brandl, I. Ott, T. Bernaś, B. Krawczyk, D. Szczukocki, K. Kowalski, *Eur. J. Inorg. Chem.* **2017**, *2*, 297.